

A new report of serpentinites from Northern Central Indian Ridge (at 6° S) – an implication for hydrothermal activity

Dwijesh Ray, Ranadip Banerjee*, Sridhar D. Iyer and Subir Mukhopadhyay¹

Geological Oceanography Division, National Institute of Oceanography, Goa 403004, India; ¹ Department of Geological Sciences, Jadavpur University, Kolkata 700 032, India

Abstract

Serpentinites from inside corner high (6°38.5'S/ 68°19.34'E) from Northern Central Indian Ridge (NCIR) are comprised mainly of high Mg-rich lizardite and chrysotile pseudomorphs with varying morphologies. 'Mesh rim', 'window', 'hourglass' and 'bastite' are the most common textures displayed by both chrysotile and lizardite. Numerous chrysotile veins in association with cross cutting magnetite veins indicate an advanced stage of serpentinisation. The higher abundance of chrysotile and lizardite suggest their close association and formation at a temperature below 250°C. Abundant 'mesh rim' and 'bastite' texture and variegated matrix reveal that the present serpentinites might have formed due to the interaction of harzburgite and seawater. Positive Eu anomaly (Eu/Eu* up to +3.38), higher La/Sm (up to 4.40) and Nb/La (up to 6.34) ratios suggest substantial hydrothermal influence during the formation of the serpentinites.

Key words: serpentinite, serpentinisation, hydrothermal alteration

1. Introduction

Ultramafic rocks provide an invaluable insight into the nature of deeper undepleted portions of the sub-ocean lithosphere and asthenosphere and also comprise a significant portion of the upper ocean crust in slow-spreading ridges. Serpentinites are commonly thought to represent hydrated mantle diapirs, uplifted and faulted extended crust, along or near a transform fault (e.g. Macdonald and Fyfe, 1985). Process of formation of serpentinites from peridotites is considered to hold one of the major clue to the low temperature metamorphism or infiltration metamorphism (Ferry, 1988). Till date, the nature of the interplay between serpentinite fault tectonics and hydrothermal discharge is poorly understood.

Exposures of serpentinites are more common in and along the slow spreading Mid-Atlantic Ridge (MAR), at the ultraslow spreading Southwest Indian Ridge (SWIR) or even at the slowest spreading Gakkel ridge, compared to the fast spreading East Pacific Rise (EPR). Serpentinised peridotites were recovered from different locations of the MAR, by dredging or drilling, including axial valley, transform fault (TF) and detachment faults (Karson et al., 1987; Bougault et al., 1990; Cannat et al., 1992; Cannat et al., 1995; Bideau et al., 1996; Escartin et al., 2003; Bach et al., 2004, Paulick et al., 2006). Ultramafic rocks were also recovered from the Garret TF, Hess Deep on the EPR and the Equador TF on the Galapagos Spreading Centre (Hebert et al., 1983).

Compared to the reports on serpentinites from MAR and EPR, those occurring along the Carlsberg-Central Indian Ridges (CR-CIR) are less known

(Iyer and Ray, 2003). Peridotites were dredged from the CR and from the Owen FZ (Hamlyn and Bonatti, 1980). Abundant ultramafics, e.g. dunites, pyroxenites were dredged from the Vityaz TF near 5°S, the Vema TF near 9°S, the Argo TF near 13°S, the Marie Celeste FZ near 17°S and from the Melville TF near 30°S and 60°E (Engel and Fisher, 1975). Other occurrences of serpentinite and peridotites along the Indian Ocean Ridge System (IOR) were reported from the SWIR, east of the Melville FZ at 62°E (Bassias and Triboulet, 1992) and along the axis of the SWIR between 52°E and 69°E (Seyler et al., 2003). Earlier reports on abyssal peridotite from CIR include only their sparse petrographic descriptions. While, their detailed mineralogy, mineral chemistry and whole-rock chemistry are still lacking for several sites of the spreading ridge segments.

Here we detail a new report on the mineralogy, crystal chemistry and whole-rock chemistry of serpentinites, recovered from one segment of the northern CIR (6°39'S/ 68°32'E, water depth 2800 m) and discussed their evolution due to the possible effect of low temperature seawater-rock interaction (hydrothermal alteration). The rock samples were dredged from a ridge-transform intersection (RTI) adjacent to Vityaz TF (Fig. 1). Thus, the present observations would address for the first time the geochemical, mineral chemical and mineralogical characters of serpentinites collected from a new tectonic setting on the CIR which is hitherto not reported till date from this ridge system.

2. Methodology

Rock thin sections were studied under plane polarised light to understand the general mineralogical and textural properties of the serpentinites.

Identification of serpentine polymorphs (mainly lizardite and chrysotile) was performed using powdered rock samples by X-ray diffraction (XRD) method. This analysis was carried out by using a Phillips 1840 diffractometer. The identification procedure was adopted from Whittaker and Zussman (1956) and PDF No.11-386 for lizardite and PDF Nos. 31-808 and 25-645 for chrysotile were used to identify serpentine species. Silicon has been used to monitor the calibration of the instrument. The operating condition was kept at 40 kv, with an operating current of 22 mA. The scanning speed was $2^{\circ}2\theta/\text{minute}$ and the scanning range was between 10 and $70^{\circ}2\theta$. Mineral chemical analyses of lizardite and chrysotile were performed using a Scanning Electron Microscope with an Energy-Dispersive X-ray spectrometer (JSM-5800LV attached with an OXFORD ISIS 300 EDS) at NIO, Goa. It was operated at 20 kV and 47 μA . Internal standard (pyrite) and glass standard (USNM 113716) was used for checking the calibration at an initial stage of the analyses. The x-ray peak counting time was kept at 100 sec and the accuracy is better than 5%. Trace and rare earth elements (REE) of bulk samples were measured using an Inductively Coupled Plasma Mass Spectrometry (ICP-MS) at NGRI, Hyderabad, following the procedure of Balaram et al. (1999). Three runs were carried out on UB-N standard (French standard) at the initial, intermediate and final stages of the analyses. Accuracy of the trace and rare earth elements (B, Cr, Co, Ni, Cu, Zn, Ga, Rb, Sr, Y, Zr, Cs, Ba, La, Th, Ce, Lu, Pb and U) was better than 5%. However, Sc and V show >12.5 and 20% accuracy, respectively. Accuracy of Yb and Tb are > 8.5%; Pr, Gd, Nd and Hf are > 10%; Sm, Eu, Dy, Ho, Er and Tm

are > 15%.

3. Results and Interpretations

Hand specimen examination of the serpentinites revealed them to be of mostly grayish to dark greenish, medium to coarse grained and with interlocking textures. Crude foliation with a shear plane was noticed on the surface of many samples together with lineation mark (slickenside) and remnants of serpentine patches. Morphologically, serpentines are platy/flaky in habit, often fibrous, with a soapy texture and mostly constituted of chrysotile and lizardite. In a few sample gabbroic dikelet intrudes within serpentinite (Fig. 2a). Lizardite sometimes occurs as elongated patches (parallel to slip direction) along the foliation (Fig. 2b) or as platy habit and chrysotile mostly occurs as vein (Figs. 2c, d). The striations on lizardite patches parallel to longer striation marks on the rock body (Fig. 2b) suggests it's possible development due to some frictional force between two rock bodies during some tectonic activity (e.g. fault movement) in that area and which is very much possible in this locality as the samples were collected from a ridge-transform fault intersection area.

Interpretation of the X-ray diffraction analyses was done using diffraction data for Lizardite 1T, chrysotile 2Mcl, and chrysotile 2Orcl, similar to what deciphered by Whittaker and Zussman (1956). Though XRD analyses provide the dominant serpentine minerals, presence of small amounts of other serpentine minerals cannot be ruled out. X-ray diffraction patterns of whole-rock

serpentinites have been illustrated in Fig. 3 to identify individual peak of the major serpentine minerals. XRD of bulk serpentinite reveal distinct peaks for both chrysotile and lizardite, more specifically 1T-lizardite (PDF No. 11-386), 2M chrysotile (PDF No. 31-808), and orthochrysotile (PDF No. 25-645; Fig. 3).

Several fine thread-like serpentine veins and veinlets occur in a criss-cross pattern, exhibiting lensoidal (even curved tapering end), 'pinch' and 'swell' structure, sometimes branching like a braided river. Different generations of veins can be ascertained by the cross-cut relationship among them (Fig. 4a). Even orthogonal and curvy veins are also noticed (Fig. 4b). In addition, the matrix shows a flaky disposition of serpentines or nicely fabricated olivine-serpentine mesh composed of fine grained lizardite and chrysotile (Fig. 4c). Orthopyroxene 'bastite' and 'window' and 'hour glass' texture (Figs. 4d, e) are also present. Further, the chrysotile veins, cutting through the early formed serpentine mesh texture were observed in some sections (Fig. 4f). Most of the relict phenocryst grains (opx) exhibit undulatory extinction. Sometimes, the primary phases might have been strained prior to the serpentinisation as revealed by the "undulatory extinction" of orthopyroxene grains caused by crystal plastic deformation (O'Hanley, 1996). Additionally, sometimes the chrysotile veins show small-scale displacement and 'bent' in 'bastite' textures indicating effect of some deformation process.

At high magnification, under the SEM, lizardite shows a flaky habit and even individual flake are noticeable (Fig. 5a, b). Spinel is the most dominant mineral (grayish white in colour under reflected light microscope), and it is the

only fresh primary mineral remaining unaltered at many places even after the extensive serpentinisation. Spinel mostly occurs as anhedral, irregular rounded, 'holly-leaf' small and vermicular aggregates. Magnetite is generally precipitated during alteration of olivine and orthopyroxenes, and commonly forms bands or "dusty" clusters of tiny opaque crystals rimming the altered primary phases. Fine disseminated stringers of magnetite sometime show a wavy pattern and warp against the pre-existing altered olivine grains. In some places, magnetites exhibit multiple branching patterns that are webbed between each other and tend to concentrate along margin or center of the serpentine mesh rims (Fig. 6a). Skeletal grains of spinel (or porphyroclasts) are also observed locally (Fig. 6b).

Mineral chemical analyses of serpentine pseudomorphs reveal an almost homogenous composition with considerably high MgO contents (avg 43.32 wt%). While their Al₂O₃ content is moderate to high (1.55 to 2.12 wt%), Cr₂O₃ content is also high (up to 1.85 wt%, Table 1). Mg/Si varies from 1.18 to 1.38 (~1.33) and Cr/Al varies from 0.34 to 0.86 (~0.48). The total FeO content is also high (4.82 wt%, Table 1).

Bulk composition of the NCIR serpentinites shows a consistently high content of MgO (44.21 wt%) and low contents of SiO₂ (35.83 wt%), TiO₂ (0.03 wt%), Al₂O₃ (0.79 wt%) and Na₂O (0.15 wt%) (Table 2). Mg# [mole Mg/(Mg+Fe)] of the present serpentinites vary from 0.87 to 0.90, which includes the normal range of whole-rock Mg# [mole Mg/(Mg+Fe)] in residual mantle peridotites from mid-ocean ridges (~0.89 to 0.92; average =~0.90-0.91, Dick, 1989). CaO content is generally < 0.06%.

The comparative major oxides values of serpentinites collected from different ridge segments of IOR are reported in Table 3. The NCIR serpentinites have high MgO (44.21), low Al₂O₃ (0.79) and CaO (0.31) contents, as compared to the previously reported average values for the CR Mg sepiolite (MgO ~19, Al₂O₃ ~3.59, CaO ~5.50), CIR Iherzolites (MgO ~34.84, CaO ~3.59, Al₂O₃ ~5.50) and SWIR serpentinitised harzburgite (MgO ~30.64, CaO ~9.41, Al₂O₃ ~1), respectively (Table 2, Engel and Fisher, 1975; Bonatti et al., 1983; Bassias and Triboulet, 1992). Generally, the Si/Mg ratio regulates Mg silicate phase generation and serpentine forms at MgO/SiO₂ ratios of 4:1 and 2:1 (Bonatti et al., 1983).

Bulk Ni content is relatively high (1189-2257 ppm) in these serpentinites, even higher than the earlier reported Ni in Iherzolite from CIR (~1300-1600 ppm, Engel and Fisher, 1975). Cr also shows a similar enrichment (423-2233 ppm), which could be due to the presence of Cr-spinel. Cr in Iherzolite reported by Engel and Fisher (from CIR) exhibit higher value (1400-3100 ppm) compared to the present serpentinites. The high field strength (HFS) elements e.g. Y and Zr have very low concentration (<10 ppm) in these serpentinites. Among the trace elements, Cr and Ni correlate positively with MgO, while V correlates negatively. In the depleted mantle-normalised multi-element plot, the present serpentinites display an enrichment of LIL elements and depletion of HFS elements and REE (Fig. 7).

The enrichment factors of the transitional metals Sc, Ti, V, Cr, Mn, Fe, Co, Ni over the mean composition of CH-carbonaceous chondrites are shown in Fig.

8a. These factors decrease regularly. All the analysed serpentinite samples are characterised by a negative Ti anomaly and a positive Ni anomaly (Fig. 8a). Fe/Mn and Fe/Cu ratios vary from 0.11-0.44 and 0.26-3.26 respectively. REE of the NCIR serpentinites have been normalised after Evensen et al. (1978). In the FeO_t-MgO-SiO₂ triangular plot the present serpentinites are seen mostly to fall within the natural chrysotile field (Fig. 8b, cf. Wicks and Plant, 1979).

Most of the samples characteristically show a moderate to strong positive Eu anomaly (Eu up to +3.38, Fig. 9a). Total REE (Σ REE) of the present serpentinite varies from 0.701 to 10.763 ppm. Samples with positive Eu anomaly have low Σ REE content (1.088-1.347). A comparison of the NCIR serpentinites with the normalised REE pattern of different hydrothermal fluid (Fig. 9b) indicates that positive Eu anomaly is common to all. Nb/La ratio also varies from 1.44 to 3.69. Both, LREE depletion [(La/Sm)_N ~0.32-1.42] as well as enrichment [(La/Sm)_N ~1.42 and 1.9] pattern are noticed in these samples. Indication of Ce, Nd and Sm enrichments were noticed in a few samples. Interestingly, a few of the samples show negative Ce anomaly (-0.44–1.045) together with HREE enrichment [(Yb/Sm)_N ~ 1.34-2.29].

4. Discussion

In hand specimen, the variegated colors on the surface of the serpentinites suggest different grades of alteration due to intense and prolonged seawater-rock interaction. The high abundances of chrysotile and lizardite

indicate their formation during the process of low temperature alteration. Oxygen and hydrogen isotope ratio of serpentinites have been frequently used to establish a range of temperatures of their formation. From, these studies it has been suggested that a mixture of oceanic lizardite and chrysotile can form at around 130⁰C to 185⁰C, while oceanic antigorite can form at around 235⁰C (Wenner and Taylor, 1973). Thus, our present mineralogical assemblages (mostly chrysotile and lizardite) also indicate a lower temperature for their formation and their paragenetic association also suggests a tendency to co-crystallise. This corroborates the study made by O'Hanley and Wicks (1995) from field, paragenetic, stable isotope, and phase equilibrium relationship and the experimental observations of Normand et al. (2002).

The water-rock mass ratio is also an important factor for the formation of the present serpentinites. Wenner and Taylor (1973) concluded that the formation of lizardite and chrysotile probably involved seawater at water/rock mass ratio >2. The high loss on ignition values (mostly 10-12 wt%) of the NCIR serpentinites is consistent with the mineralogy of the samples and indicate substantial interaction between the seawater and peridotites.

Distribution of magnetite often correlates with the degree of serpentinisation, as reflected by the alteration hues of serpentinites in hand specimen. At advanced stages of serpentinisation, the magnetite migrates out of the mesh or hour glass textural units into cross-cutting lenses and veinlets and the rock usually appears as green or often pale green in colour (Fig. 4; Wicks and Whittaker, 1977). This suggests that the formation of chrysotile veins

occurred subsequent to formation of lizardite. In addition, magnetite texture also depends on the degree of serpentinisation. Magnetite initially formed as small discrete grains within the textural units, but migrated during pervasive serpentinisation to form coarser grains and stringers and finally formed even coarser cross-cutting lenses and veins as serpentinisation progressed. Abundant cross cutting magnetite veins might have resulted due to a late tectonic upliftment of the oceanic crust, which facilitated to accommodate the opening of vein space and their subsequent filling by serpentine minerals. Thus the tectonic processes facilitated the circulation of high temperature fluid and subsequently the fluid was transported through the veins. This is also exemplified by the presence of chrysotile veinlets post-dating the early serpentine veins (Fig. 4f).

Serpentine mineral with high MgO (up to 50 wt%) in association with high Al_2O_3 (up to 2.12 wt%) and Cr_2O_3 (up to 1.85 wt%) content suggest that the analyzed serpentine minerals are mostly pseudomorph of orthopyroxene (i.e. bastite). The high MgO and Fe_2O_3 , contents of the bulk rocks accompanied by their low contents of SiO_2 and CaO suggest that the parent rock was possibly harzburgite (olivine and orthopyroxene dominant) while the low Al_2O_3 and TiO_2 contents support a residual nature of the NCIR peridotite (Table 2). The low Mg# [mole Mg/(Mg+Fe)] in peridotite (<0.89) could be due to metasomatic changes in Fe/Mg because of hydrothermal alteration, olivine crystal fractionation, or reaction of migrating melt with residual mantle peridotite. Preferential loss of Ca during serpentinisation processes could also prompt low CaO values of the present peridotite. The low Ba content (6-28 ppm) in the bulk rock is also in

accord with the serpentinite composition and decreases as the degree of serpentinisation increases. Also the present harzburgites display a distinct major element characteristic with their high MgO and FeO_t content as compared to lherzolite, Mg sepiolite or serpentinised harzburgite from other locations of IOR (Table 3).

Positive Eu anomaly of the NCIR serpentinites cannot be attributed to the plagioclase accumulation as the parent rock is plagioclase free (mostly residual in nature) and Sr values are very low (Table 2). The enrichment of Eu over other REEs may have been produced under pronounced reducing conditions during seawater-ultramafic rock interaction. Also, the low Ba (Ba decreases as serpentinisation increases) as well as Y and Zr content in these serpentinites are in good agreement with the enrichment trend of Eu. The observed positive Eu anomaly (Fig. 9b) is in good agreement with the REE content of hydrothermal fluid collected from different locales at MAR, suggesting substantial hydrothermal input during the formation processes of the NCIR serpentinites. A possible interaction of Eu-enriched hydrothermal fluids with the present serpentinites could have helped to increase the Eu content in these rocks (German et al., 1999; Paulick et al., 2006). Thus, high value of Nb/La ratio (up to 6.34) in association with the highest positive Eu anomaly (Eu/Eu* up to +3.38) suggests the possibility of a higher degree of hydrothermal input and this is further supported by higher La/Sm values (e.g. up to 4.40). Negative Ce anomaly and HREE enrichments attest to the ongoing rock-seawater interaction, a post emplacement process affecting the serpentinites.

Serpentine mineralogy e.g. mainly co-existence of lizardite and chrysotile favor prolonged low temperature (~250°C) alteration. Further, it suggests that the process of serpentinisation in the study area was probably initiated at a low temperature and at a low to moderate pressure (generally < 2kb, cf. Mevel, 2003). This pervasive serpentinisation favors formation of extensive mesh texture, characterised by structureless serpentine replacing olivine, and pseudomorphs of lizardite in addition to formation of orthopyroxene 'bastite' texture (Figs. 4c, d). In addition, the abundant later formed magnetite strings along with obliteration of original textures indicate a higher degree of serpentinisation (Fig. 6a).

The different morphotypes of serpentine veins indicate that intense alteration occurred during a prolonged period of rock-seawater interaction. In addition, abundant cross cutting vein might have resulted due to late tectonic upliftment of the ocean crust, which facilitated to accommodate the opening of vein space and their subsequent fill up by serpentine minerals and this process is similar to the MARK serpentinites reported from MAR (Dilek et al., 1997). Such processes may have facilitated the circulation of high temperature fluid and it's subsequent transport through numerous veins. This is also exemplified by the presence of chrysotile veinlets post-dating the early serpentine veins.

5. Summary

Our findings on the occurrence of serpentinites at Vityaz TF reveal that the mineralogical assemblages of these rocks are dominated by the occurrence of

lizardite and chrysotile, associated with magnetite, which might have developed during a prolonged low temperature ($\sim 250^{\circ}\text{C}$) seawater-rock interaction. Both high Al_2O_3 and Cr_2O_3 contents of bastite supports their formation from orthopyroxene due to long term serpentinization process. Positive Eu anomaly also suggests at some point of time reducing hydrothermal fluids acted upon these serpentinites during and after their emplacement. Residual characters of present serpentinites is revealed by their low bulk Ti content (bulk $\text{TiO}_2 \sim 0.03\%$) and lack of plagioclase (bulk Sr < 4 ppm). The implications of serpentinisation at this part of the CIR suggest a possibility of occurrence of an active hydrothermal discharge nearby which could have a similarity with other known ultramafic-hosted hydrothermal field, e.g. Rainbow in MAR. Additional study is required in this area to locate the exact hydrothermal discharge zone.

Acknowledgements

We thank the Director, NIO, for permission to publish the manuscript. Ship time was provided by the Department of Ocean Development, New Delhi. This research is partly funded by ONR grant no. 0014-97-1-0925 and CSIR Network Programme (COR 0006) on Indian Ocean ridges. We appreciate the help extended by the Captain and crew members onboard ORV Sagar Kanya and other colleagues during the sampling operations. DR is grateful to CSIR, New Delhi, for financial support in the form of a Senior Research Fellowship. We thank Dr. H J Wang for his critical comments and suggestions to improve the manuscript. This is NIO's contribution #.....

References:

Balaram, V., Gnaneshwara Rao, T., and Anjaiah, K.V., 1999. International proficiency tests for analytical geochemistry laboratories: an assessment of accuracy and precision in routine geochemical analysis. *J. Geol. Soc. India*, 53: 417-423.

Bach, W., Garrido, C.J., Paulick, H., Harvey, J. and Rosner, M., 2004. Seawater-peridotite interaction: first insights from ODP Leg 209, MAR 15°N. *Geochem. Geophys. Geosyst.*, 5(9): doi 10.1029/2004 GC000744.

Bassias, Y. and Triboulet, C., 1992. Petrology and P-T-t evolution of the South West Indian Ridge Peridotites, A case study: east of Melville fracture zone at 62°E. *Lithos*, 28: 1-19.

Bideau D. et al., 1996. Submersible investigation of highly contrasted magmatic activities recorded on two segments of the Mid-Atlantic Ridge near 34°52'N and 33°55'N. *Inter Ridge News*, 5: 9-14.

Bonatti, E., Simmons, E.C., Breger, D., Hamlyn, P.R., and Lawrence, J., 1983. Ultramafic rock/seawater interaction in the oceanic crust: Mg silicate (sepiolite) deposit from the Indian Ocean floor. *Earth Planet. Sci. Lett.*, 62 : 229-238.

Bougalt H. et al., 1990. Campagne RIDELENTE: structure de la dorsale Atlantique-Heterogeneite du manteau et hydrothermalisme. *Oceanologica Acta* 10: 366-381.

Burkhard, D.J.M., 1992. Accessory chromium spinels: Their existence and alteration of serpentinites. *Geochim. Cosmochim. Acta*, 57: 1297-1306.

Cannat, M., Bideau, D., and Bougalt, H., 1992. Serpentinised peridotites and gabbros in the Mid-Atlantic Ridge axial valley at 15°37'N and 16°52'N. *Earth Planet. Sci. Lett.*, 109: 87-106.

Cannat M. et al., 1995. Thin crust, ultramafic exposures, and rugged faulting patterns at the Mid-Atlantic Ridge (22-24°N). *Geology*, 23: 49-52.

Charlou, J.-L., J.P. Donval, Fouquet, Y., Jean Batiste, P., and Holm, N., 2002. Geochemistry of high H₂ and CH₄ vent fluids issuing from ultramafic rocks at the Rainbow hydrothermal field (36°14'N, MAR). *Chem. Geol.*, 191: 345-359.

Coogan, L.A., Wilson, R.N., Gillis, K.M., and Macleod, C.J., 2001. Near solidus evolution of oceanic gabbros: Insights from amphibole geochemistry. *Geochim. Cosmochim. Acta*, 65: 4339-4357.

Dick, H.J.B., 1989. Abyssal peridotites, very slow spreading ridges and oceanic ridges and ocean ridge magmatism. In: Saunders, A.E., and Norris, M.J. (eds.), *Magmatism in the Ocean Basins*. Geological Society of America, Boulder, Colorado, 71-105.

Dilek, Y., Coulton, A. and Hurst, S.D., 1997. Serpentinisation and hydrothermal veining in peridotites at site 920 in the MARK area. In: Karson, J.A., Cannat, M., Miller, D.J., and Elthon, D. (eds.), *Proceedings of the Ocean Drilling Program, Scientific Results*, 153: 35-59.

Douville, E., Charlou, J.L., Oelkers, E.H., Bienvenu, P., Jove Colon, C.F., Donval, J.P., Fouquet, Y., Prieur, D., and Appriou, P., 2002. The rainbow vent fluids (26°14'N, MAR): the influence of ultramafic rocks and phase separation on trace metal content in Mid-Atlantic Ridge hydrothermal fluids. *Chem. Geol.*, 184: 37-48.

Engel, C. G., and Fisher, R.L., 1975. Granitic to ultramafic rock complexes of the Indian ocean Ridge System, western Indian Ocean. *Bull. Geol. Soc. Am.*, 86: 1553-1578.

Escartin, J., Mevel, C., MacLeod, C.J., and McCaig, A.M., 2003. Constraints on deformation condition and the origin of oceanic detachments: The mid Atlantic ridge core complex at 15°45'N. *Geochem. Geophys. Geosyst.* 4(8): doi: 10.1029/2002GC000472.

Evensen, N.M., Hamilton, P.J., and O'Nions, R.K., 1978. Rare earth abundances in chondritic meteorites. *Geochim. Cosmochim. Acta*, 42: 1119-1212.

Ferry, J.M., 1988. Infiltration-driven metamorphism in northern New England. *J. Petrol.*, 29: 1121-1159.

German, C. R., Hergt, J., Palmer, M. R., and Edmond, J. M., 1999. Geochemistry of a hydrothermal sediment core from the OBS vent-field, 21°N East Pacific Rise. *Chem. Geol.*, 155(1-2): 65-75.

Hamlyn, P.R., and Bonatti, E., 1980. Petrology of mantle derived ultramafics from the Owen fracture zone, northwest Indian Ocean: Implications for the nature of the oceanic upper mantle. *Earth Planet. Sci. Lett.*, 48: 65-79.

Hebert, R.D., Bideau, D., and Hekinian, R. 1983. Ultramafics and mafic rocks from the Garret transform fault near 13°30'S on the East Pacific Rise: Igneous Petrology. *Earth Planet. Sci. Lett.* 65: 107-125.

Iyer, S.D., and Ray, D., 2003. Structure, tectonic and petrology of mid-oceanic ridges and the Indian scenario. *Curr. Sci. (Special Section on Mid-Oceanic Ridges)*, 85: 277-289.

Janecky, D.R., and Seyfried Jr., W.E., 1986. Hydrothermal serpentinisation of peridotite within the oceanic crust: Experimental investigations of mineralogy and major element chemistry. *Geochim. Cosmochim. Acta*, 50: 1357-1378.

Karson et al., 1987. Along axis variations in seafloor spreading in the MARK area. *Nature*, 328: 681-685.

Kelley et al., 2001. An off-axis hydrothermal vent field near the Mid-Atlantic ridge at 30 degrees north. *Nature*, 412: 127-128.

Macdonald, A.H., and Fyfe, W.S., 1985. Rate of serpentinisation in seafloor spreading. *Tectonophysics*, 116: 123-135.

Mével, C., 2003. Serpentinisation of abyssal peridotite at mid ocean ridges. *C. R. Geosciences*, 335: 825-852.

Normand, C., Williams-Jones, A.E., Martin, R.F., and Vali, H., 2002. Hydrothermal alteration of olivine in a flow-through autoclave: nucleation and growth of serpentine phases. *Am. Mineral.*, 87: 1699-1709.

O'Hanley, D. S., and Wicks, F.J., 1995. Conditions of formation of lizardite, chrysotile and antigorite, Cassiar, British Columbia. *Can. Mineral.*, 33: 753-773.

O'Hanley, D.S., 1996. Serpentinities, Oxford University Press, New York, 277pp.

Paulick H., Bach, W., Godard, M., De Hoog, J.C.M., Suhr, G., and Harvey, J., 2006. Geochemistry of abyssal peridotites (Mid-Atlantic Ridge, 15°20'N, ODP Leg 209): Implication for fluid/rock interaction in slow spreading environments. *Chem. Geol.*, 234:179-210.

Seyler, M., Cannat, M., and Mével, C., 2003. Evidence for major-element heterogeneity in the mantle source of abyssal peridotites from the Southwest Indian Ridge (52° to 68°E), *Geochem. Geophys. Geosyst.*, 4(2): doi: 10.1029/2002GC000305.

Sun, S.S., and McDonough, W.F., 1989. Chemical and isotope systematics of ocean basalts: implications for mantle composition and processes, In: Saunders, A.D., and Norry, M.J.(eds.). *Magmatism in the Ocean Basins*. Geological Society of London Special Publication, 42: 313-345.

Wenner, D.B., and Taylor, H.P., 1973. Oxygen and hydrogen isotope studies of serpentinisation of ultramafic rocks. *Am. J. Sci.*, 273: 207-239.

Whittaker, E.J.W., and Zussman, J., 1956. The characterization of serpentine minerals by x-ray diffraction, *Mineral. Mag.*, 233: 107-126.

Wicks, F.J., and Whittaker, E.J.W., 1977. Serpentine textures and serpentinisation. *Can. Mineral.*, 15: 459-488.

Wicks, F.J., and Plant, A.G., 1979. Electron-microprobe and x-ray microbeam studies of serpentine textures. *Can. Mineral.*, 17: 785-830.

Table 1. Representative EDS analyses of NCIR serpentine minerals.

Oxides (wt%)	Grain 1	Grain 2	Grain 3	Grain 4	Grain 5	Grain 6	Grain 7	USNM (std)
N=average of 3 spots								
SiO ₂	49.17	47.96	47.79	48.37	50.38	49.55	47.51	±1.53
Al ₂ O ₃	1.57	1.86	2.14	1.85	1.85	1.55	2.12	±0.58
Fe ₂ O ₃	4.21	4.72	5.01	4.30	5.35	4.97	4.77	±1.46
*FeO _t	3.79	4.25	4.51	3.87	4.82	4.47	4.29	-----
MgO	43.69	44.20	43.83	43.83	40.59	42.93	44	±0.24
Cr ₂ O ₃	1.19	1.26	1.22	1.01	1.85	1.01	1.61	±0.58
Sum (recalculated to 100)	99.57	99.52	99.49	98.92	99.47	99.51	99.53	

*FeO_t calculated as FeO+0.9*Fe₂O₃.

Table 2. Representative major, trace and REE contents of the NCIR serpentinites.

Oxides (wt%)	1	2	3	4	5	6	7
SiO ₂	33.43	34.78	33.74	39.09	38.74	37.48	38.58
TiO ₂	0.06	0.02	0.03	0.02	0.01	0.01	0.01
Al ₂ O ₃	1.23	0.89	0.96	0.80	0.66	0.7	0.65
FeO _t	9.02	9.41	8.47	9.50	10.12	10.84	10.76
MnO	0.16	0.16	0.14	0.15	0.16	0.2	0.2
MgO	42.87	42.22	42.84	48.64	47.51	48.28	47.62
CaO	0.02	0.03	0.06	0.02	1.33	0.01	0.02
Na ₂ O	0.13	0.13	0.2	0.18	0.13	0.18	0.18
K ₂ O	0.01	0.02	0.01	0.01	0.01	0.01	0.01
P ₂ O ₅	0.02	0.01	0.02	0.03	0.03	0.03	0.02
Element (ppm)							
Sc	15.58	15.531	15.87	15.72	16.17	16.4	16.25
Cr	1453.47	1443.09	1699.11	1443.72	1728.07	1678.09	1613.56
Co	111.76	103.09	82.64	87.29	109.55	87.57	92.48
Ni	1382.35	2256.54	1599.38	1495.86	2207.07	1911.40	1812.63
Cu	9.33	11.20	17.49	24.95	11.99	141.89	380.98
Zn	48.47	50.27	53.60	49.62	48.83	127.17	155.1
Ga	2.07	1.76	1.28	1.72	1.44	1.53	1.6
Rb	0.42	0.59	0.33	0.37	0.40	0.51	0.48
Sr	1.65	2.90	3.40	2.10	56.76	2.61	4.28
Y	2.62	1.24	0.56	0.61	0.36	0.47	0.45
Zr	2.61	2.05	1.17	2.39	1.50	1.04	1.51
Nb	0.37	0.32	0.18	0.29	0.33	0.17	0.17
Cs	0.02	0.02	0.01	0.01	0.01	0.02	0.02
Ba	16.78	17.43	11.97	17.71	13.72	14.90	17.14
La	0.26	0.19	0.10	0.20	0.09	0.11	0.15
Ce	0.82	0.30	0.13	0.17	0.14	0.29	0.34
Pr	0.12	0.05	0.02	0.03	0.02	0.03	0.04
Nd	0.67	0.27	0.11	0.14	0.08	0.15	0.14
Sm	0.18	0.08	0.04	0.04	0.02	0.04	0.05
Eu	0.06	0.03	0.01	0.01	0.01	0.05	0.05
Gd	0.37	0.13	0.04	0.5	0.03	0.05	0.05
Tb	0.05	0.02	0.008	0.01	0.01	0.01	0.01
Dy	0.32	0.16	0.04	0.05	0.03	0.05	0.04
Ho	0.07	0.03	0.01	0.01	0.01	0.01	0.01
Er	0.19	0.14	0.04	0.07	0.03	0.04	0.05
Tm	0.42	0.27	0.08	0.15	0.07	0.11	0.11
Yb	0.20	0.14	0.06	0.08	0.05	0.05	0.05
Lu	0.03	0.02	0.01	0.02	0.01	0.01	0.01

Table 3. Major element comparison of serpentinites and serpentinitised peridotites from different locations of Indian Ocean Ridge System.

Location and major element oxides (wt%)	NCIR ¹ Present study	CIR ² (17°03'S/ 66°52'E)	CR ³ (11°44'N/ 57°43'E)	SWIR ⁴ (30°S/ 62°E)
n=no. of analyses	18	1	2	8
SiO ₂	35.83	44.15	51.95	36.72
TiO ₂	0.03	0.03	0.06	0.07
Al ₂ O ₃	0.79	3.59	1.00	9.41
FeO _t	10.05	6.67	4.85	7.74
MnO	0.17	0.10	0.23	0.16
MgO	44.21	34.84	19.00	30.64
CaO	0.31	5.50	0.89	1.00
Na ₂ O	0.15	0.19	1.05	0.56
K ₂ O	0.02	<0.01	0.55	0.09
P ₂ O ₅	0.03	n.a.	n.a.	0.04

¹Serpentinised harzburgite (present study)

²Lherzolie, Engel and Fisher (1975)

³Sepiolite, Bonatti et al. (1983)

⁴Serpentinised peridotite, Bassias and Triboulet (1992)

Figure captions

Fig 1. Sampling location on the NCIR. Filled square represents the dredge location, south of the Vityaz TFat ridge-transform intersection (RTI). Thin lines represent the TF and bold lines are ridge segment. CR~ Carlsberg Ridge, NCIR~ Northern Central Indian ridge, CIR~ Central Indian Ridge, RTJ~ Rodriguez Triple Junction, SWIR~ Southwest Indian Ridge and SEIR~ Southeast Indian Ridge. Depth contour map scale 1: 5000000.

Fig 2. Plate showing the hand specimens of the NCIR serpentinites.

- a. Intrusion of gabbroic dikelet (G) within serpentinite. Coin diameter ~2.3 cm.
- b. White patchy lizardite (Lz). Length of wooden stick is ~ 6.1 cm.
- c. Platy lizardite (Lz). Bar scale ~1 cm.
- d. Vein chrysotile (Ctl)

Fig 3. X-ray diffractogram of whole-rock serpentinite (Ctl ~chrysotile; Lz ~ lizardite).

Fig 4. Photomicrograph of the NCIR serpentinites taken in cross-polarized light. Scale bar in mm and objective within the parenthesis

- a. Chrysotile veins (Ctl) crosscutting each other. V1 is early formed, V2 intermediate and V3 is the late formed.
- b. Different morphotypes of veins (e.g. meandering and orthogonal) and mesh textures (after Ol)
- c. Mesh-rim texture formed by chrysotile-lizardite
- d. Bastitic texture (after Opx)
- e. Chrysotile vein cross-cutting the early formed mesh-rim texture
- f. Hourglass texture in the serpentinite matrix

Fig 5a. SEM of flaky lizardite

- b. An enlarged view of the 5a.

Fig 6. Photomicrographs of the NCIR serpentinites. Scale bar in mm and objective within the parenthesis.

- a. Anastomising late magnetite vein under transmitted light (crossed nicol)
- b. Spinel porphyroclast under reflected light

Fig 7. Depleted mantle-normalised multielement plot (depletion MORB data are from Sun and McDonough (1989)

Fig 8a. Spidergram of chondrite normalized transitional element.

- b. FeO_t-MgO-SiO₂ ternary plot of the lizardite and chrysotile studied.

Fig 9a. Spidergram of chondrite normalised REE. REE normalization factors are

from Evensen et al. (1978).

b. A comparative plot of REE from different hydrothermal vent fluid, seawater and present serpentinite (avg. data). Except for the serpentinite, all REE data are from Douville et al. (2002).

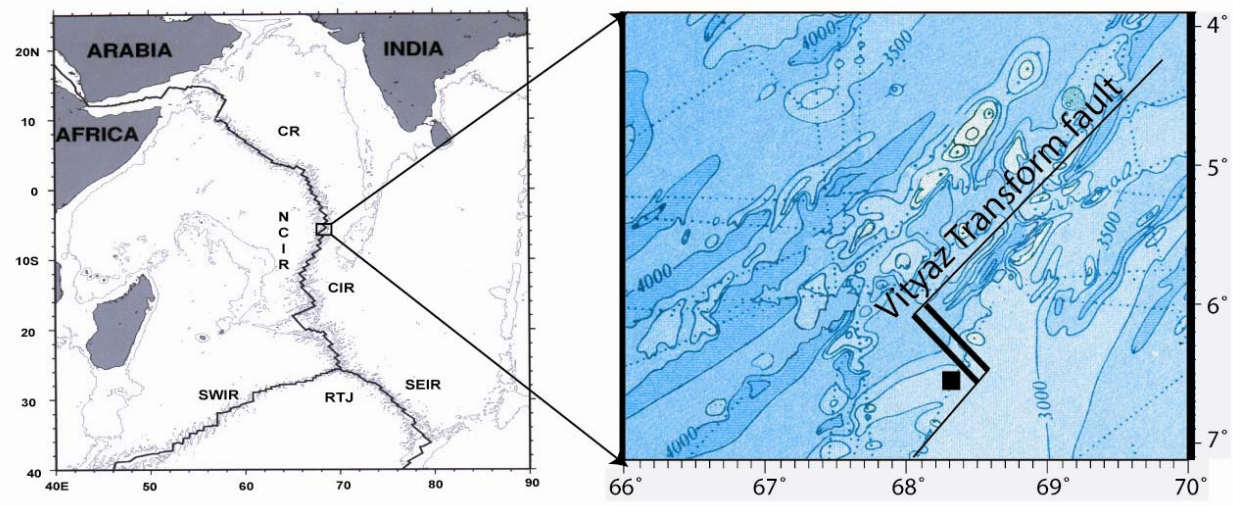


Fig 1. Sampling location on the NCIR. Filled square represents the dredge location, south of the Vityaz TFat ridge-transform intersection (RTI). Thin lines represent the TF and bold lines are ridge segment. CR~ Carlsberg Ridge, NCIR~ Northern Central Indian ridge, CIR~ Central Indian Ridge, RTJ~ Rodriguez Triple Junction, SWIR~ Southwest Indian Ridge and SEIR~ Southeast Indian Ridge. Depth contour map scale 1: 5000000.

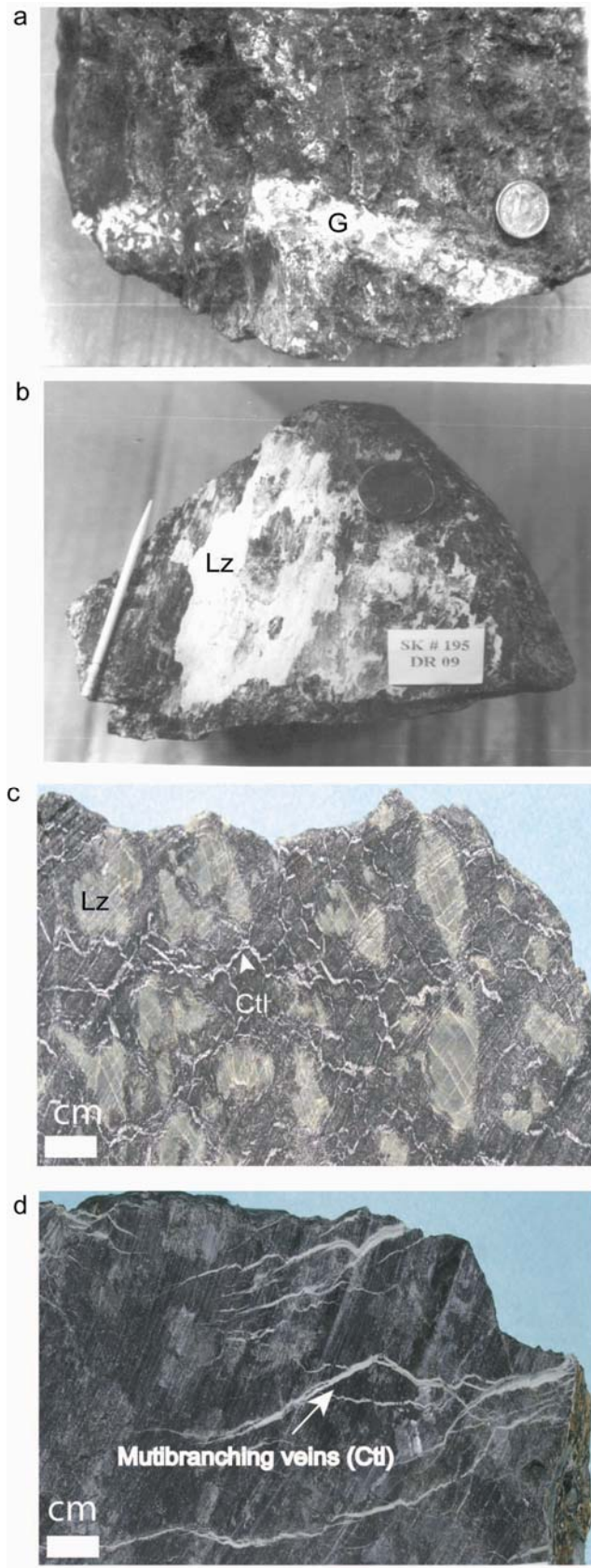


Fig 2. Plate showing the hand specimens of the NCIR serpentinites. (a). Intrusion of gabbroic dikelet (G) within serpentinite. Coin diameter ~2.3 cm. (b). White patchy lizardite (Lz). Length of wooden stick is ~6.1 cm. (c). Platy lizardite (Lz). Bar scale ~1 cm. (d). Vein chrysotile (Ctl)

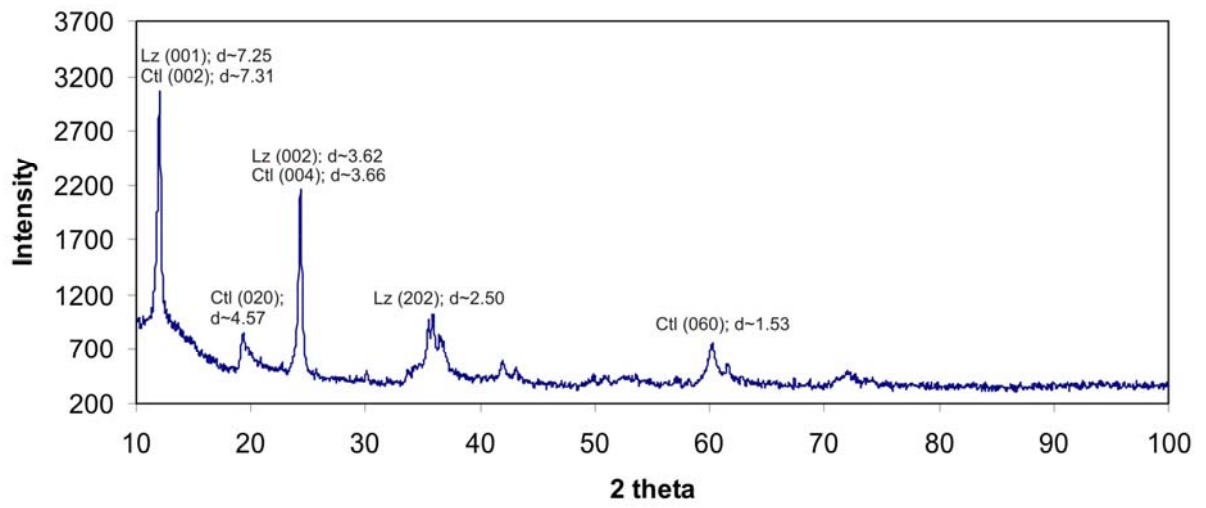


Fig 3. X-ray diffractogram of whole-rock serpentinite (Ctl ~chrysotile; Lz ~ lizardite).

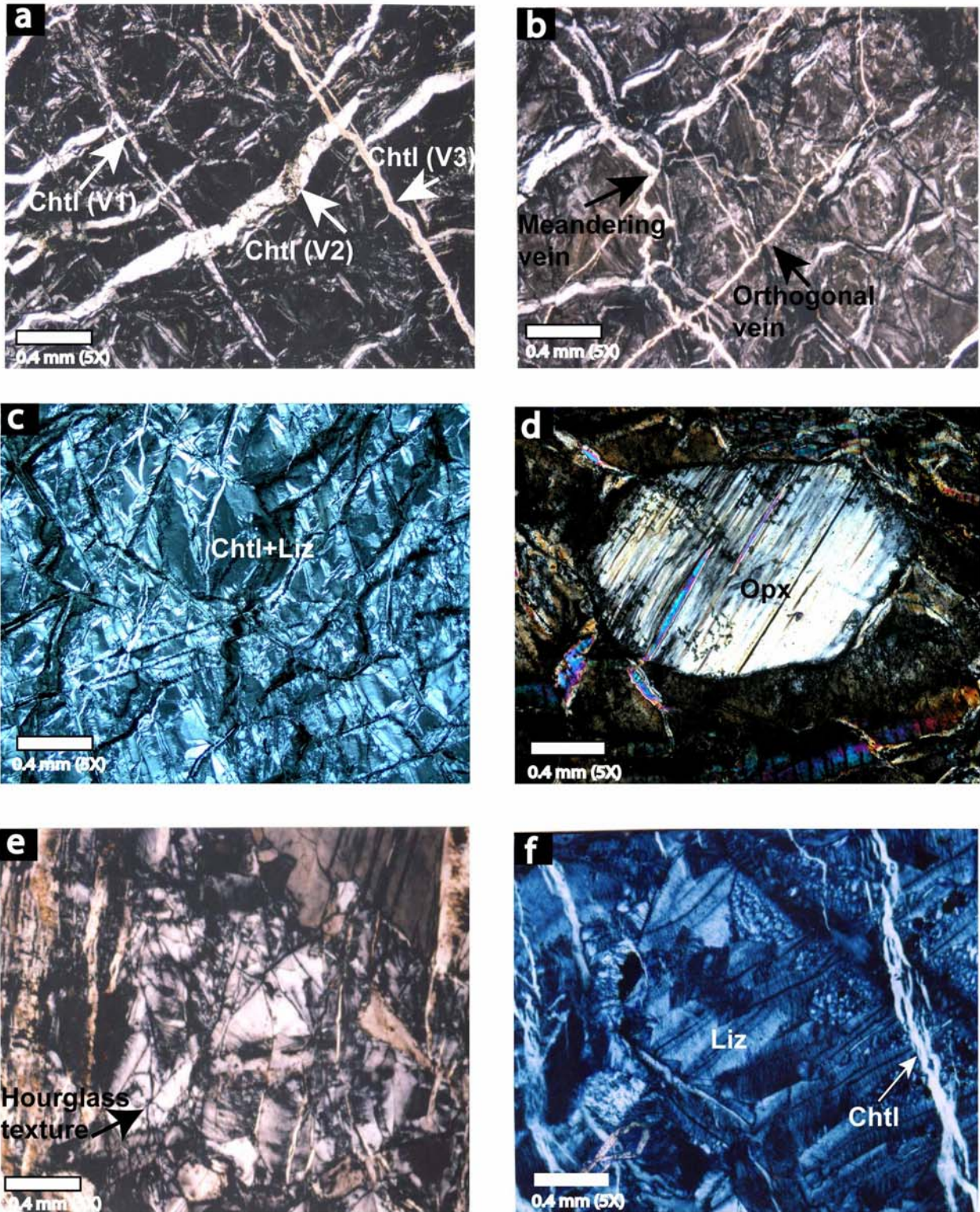


Fig 4. Photomicrograph of the NCIR serpentinites taken in cross-polarized light. Scale bar in mm and objective within the parenthesis
 (a). Chrysotile veins (Chtl) crosscutting each other. V1 is early formed, V2 intermediate and V3 is the late formed. (b). Different morphotypes of veins (e.g. meandering and orthogonal) and mesh textures (after OI) (c). Mesh-rim texture formed by chrysotile-lizardite (d). Bastitic texture (after Opx) (e). Chrysotile vein cross-cutting the early formed mesh-rim texture (f). Hourglass texture in the serpentinite matrix

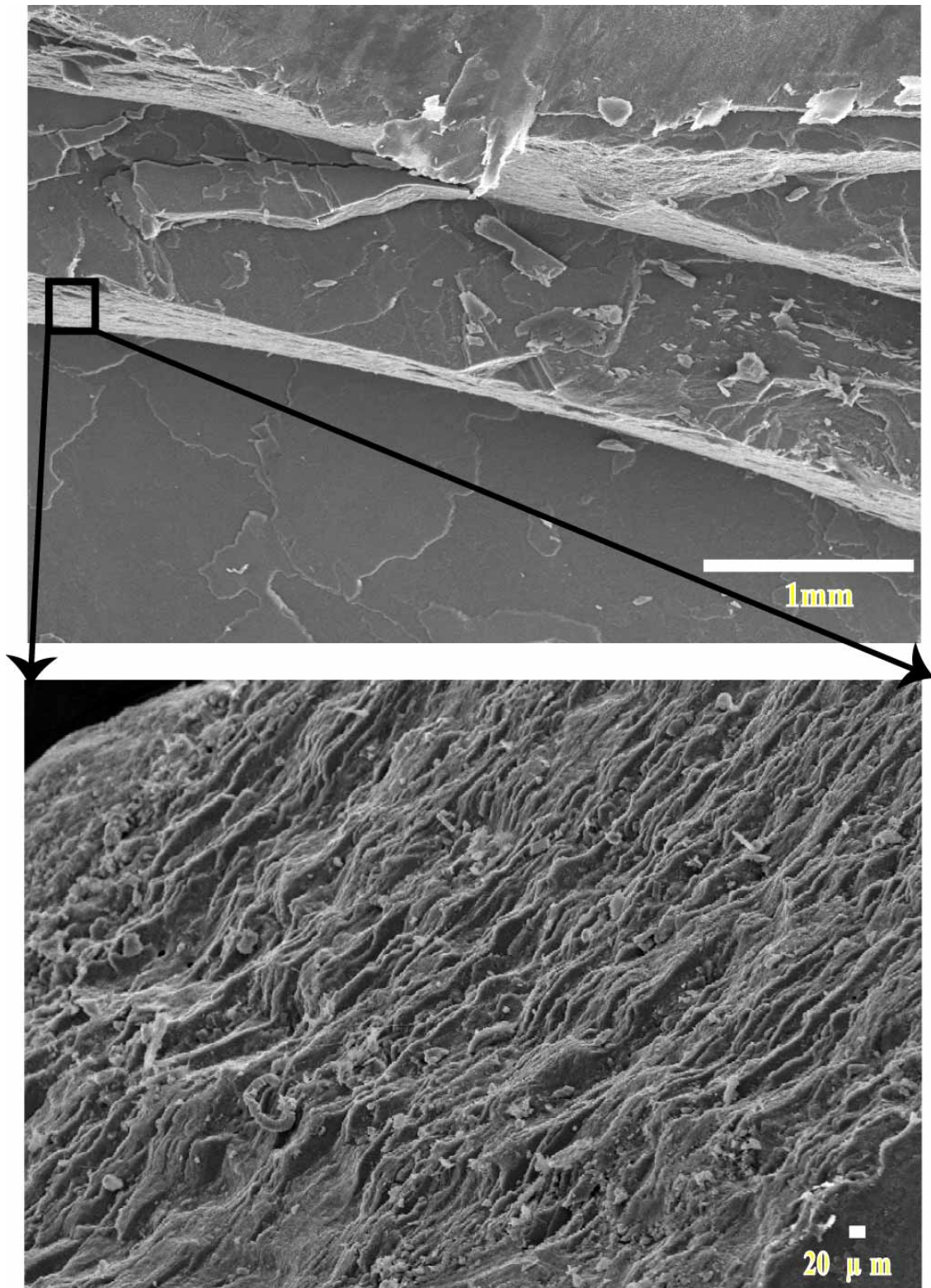


Fig 5

- a. SEM of flaky lizardite
- b. An enlarged view of the 5a.

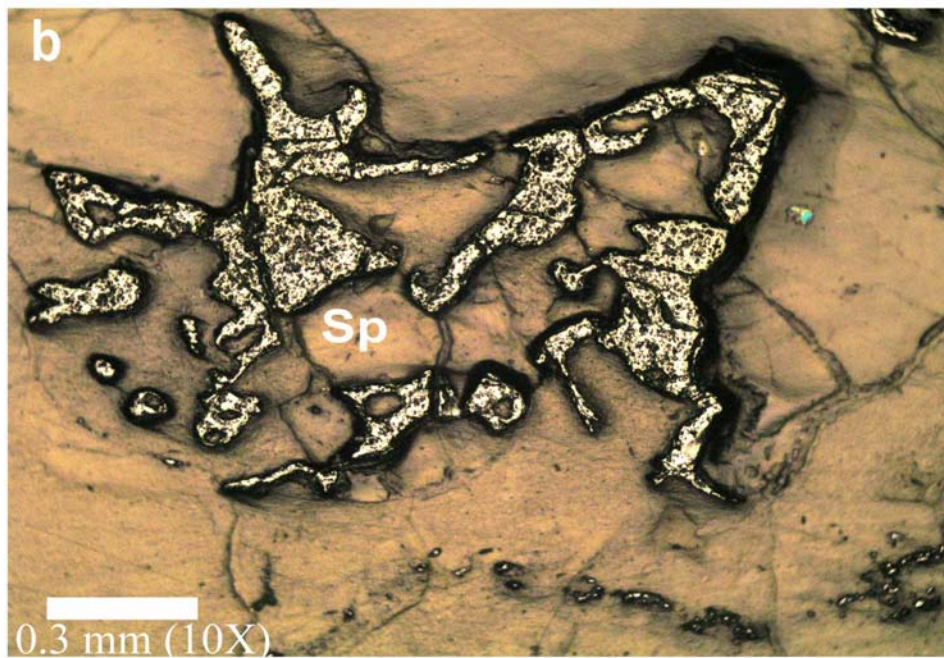
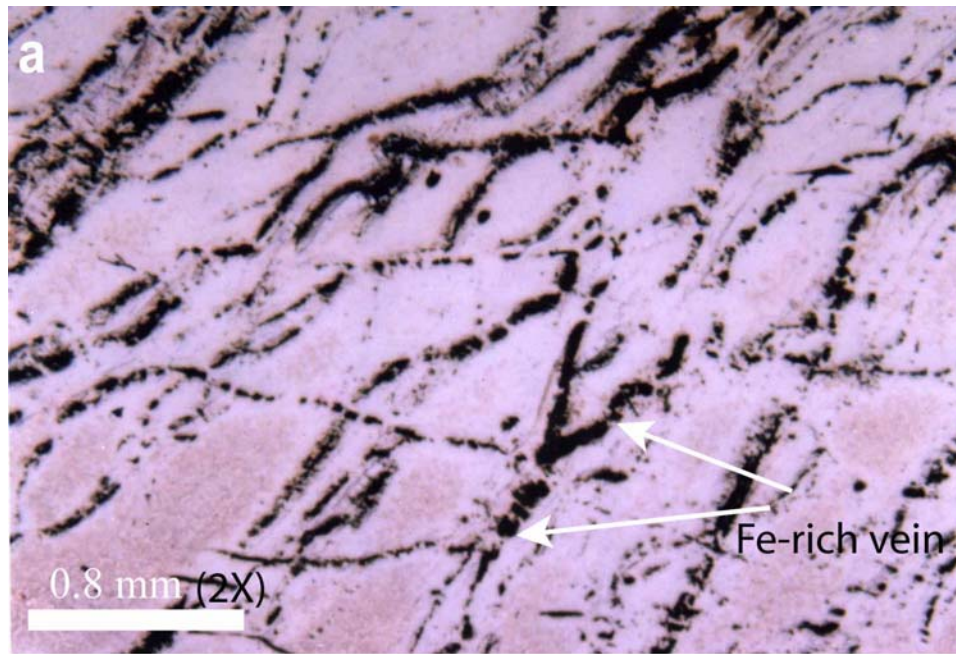


Fig 6. Photomicrographs of the NCIR serpentinites. Scale bar in mm and objective within the parenthesis.

- a. Anastomosing late magnetite vein under transmitted light (crossed nicol)
- b. Spinel porphyroblast under reflected light

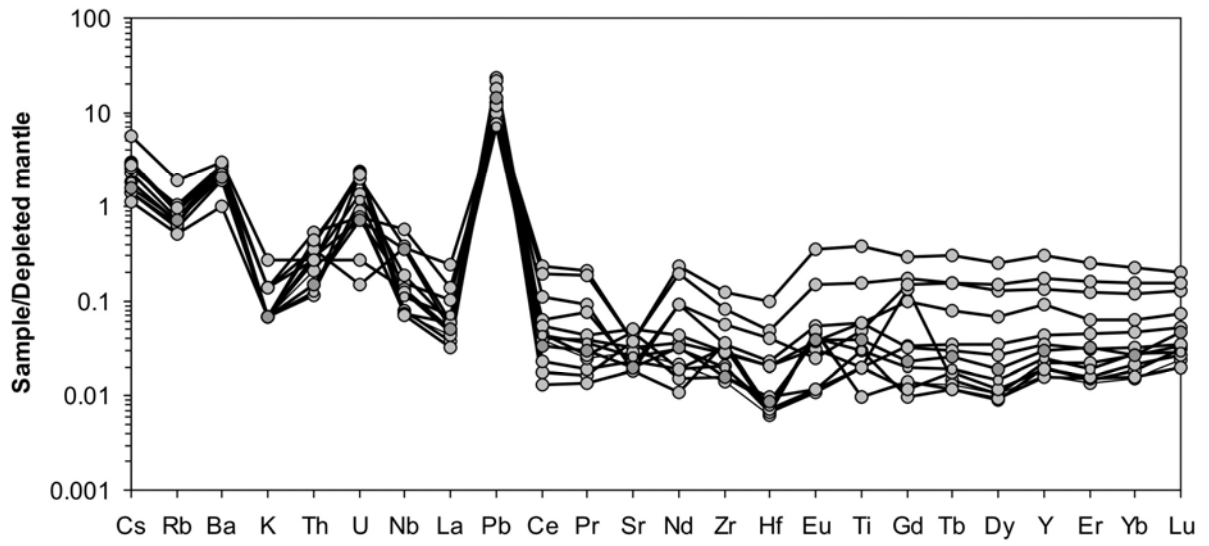
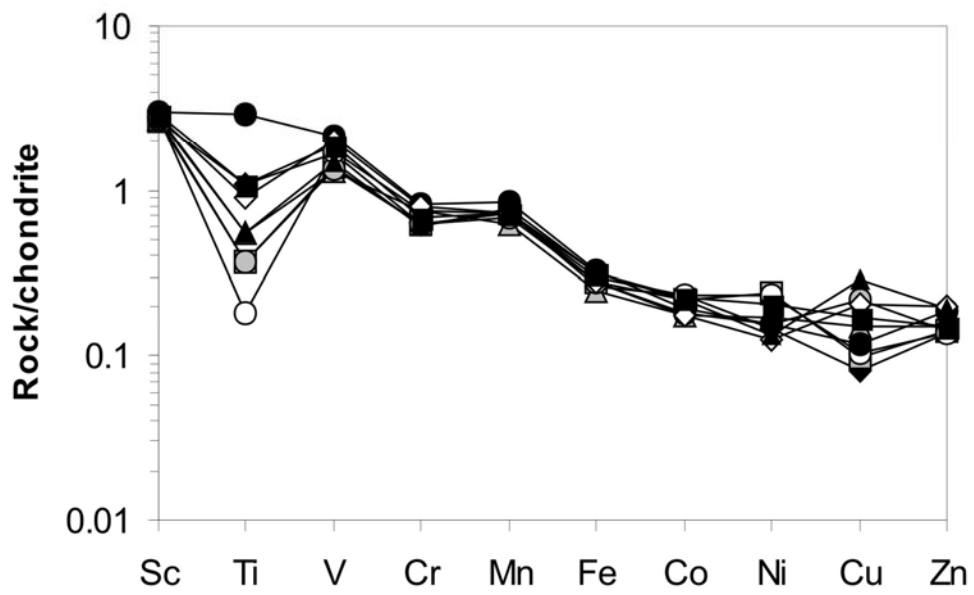


Fig 7. Depleted mantle-normalised multi-element plot (depletion MORB data are from Sun and McDonough (1989))

A



B

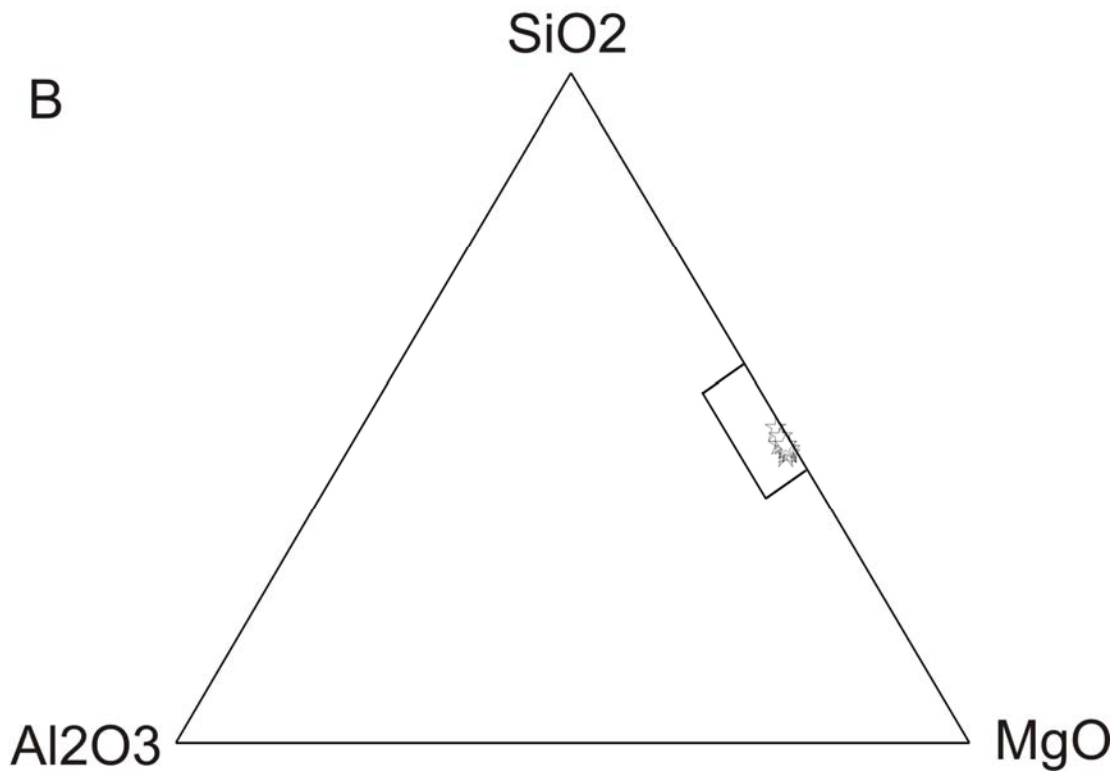


Fig 8a. Spidergram of chondrite normalized transitional element.

b. FeO-MgO-SiO₂ ternary plot of the lizardite and chrysotile studied.

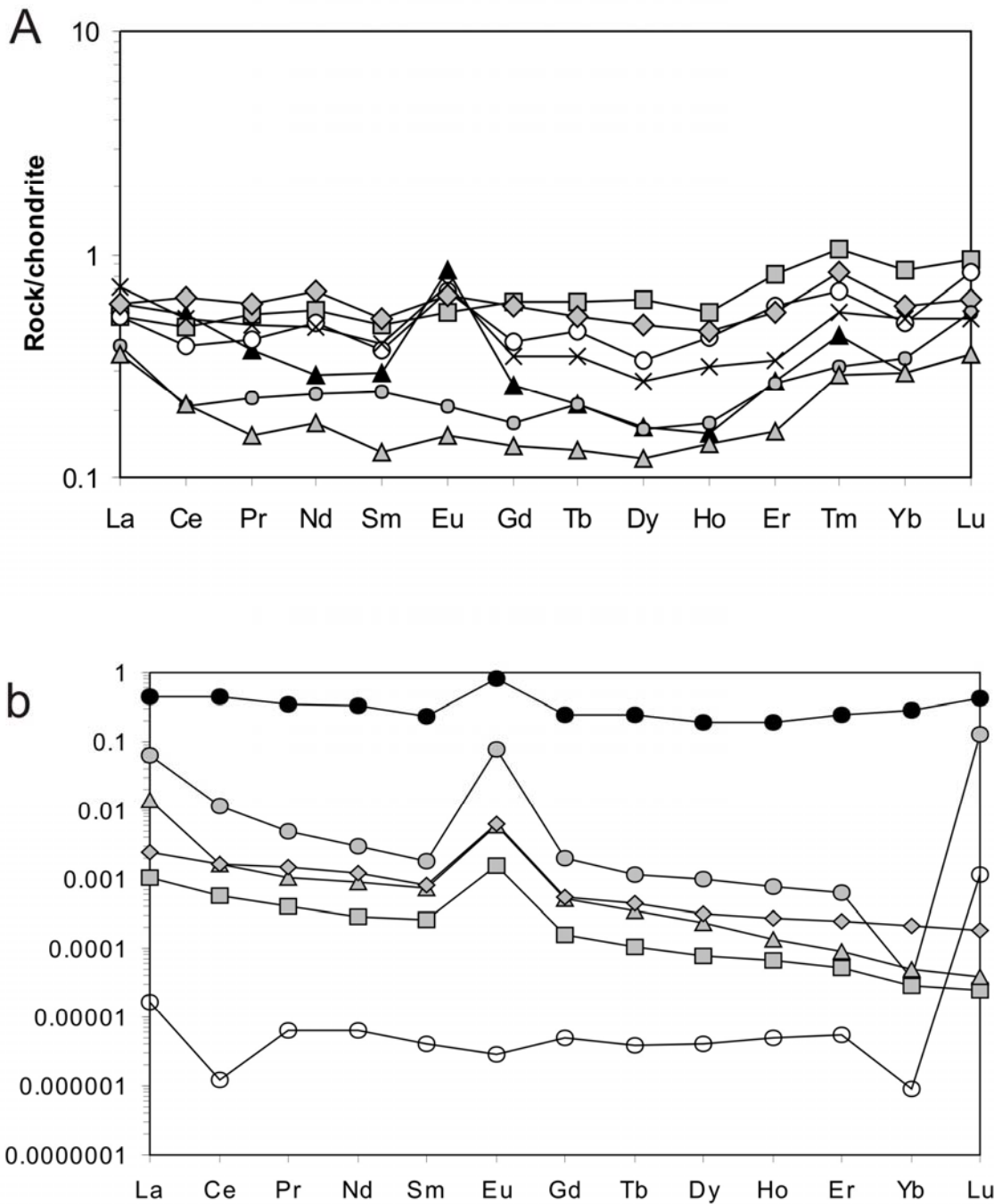


Fig 9a. Spidergram of chondrite normalised REE. REE normalization factors are from Evensen et al. (1978).

b. A comparative plot of REE from different hydrothermal vent fluid, seawater and present serpentinite (avg. data). Except for the serpentinite, all REE data are from Douville et al. (2002).